



Effect of Addition of K, Rh and Fe Over Mo/HZSM-5 on Methane Dehydroaromatization Under Non-oxidative Conditions

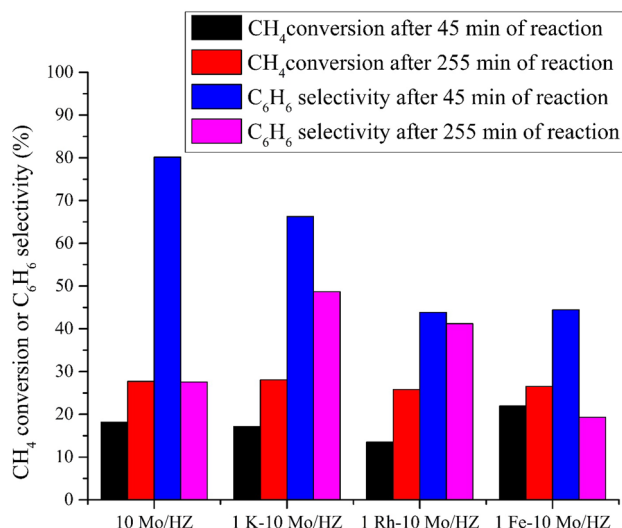
Vaidheeshwar Ramasubramanian¹ · Daniel J. Lienhard¹ · Hema Ramsurn¹ · Geoffrey L. Price¹

Received: 28 November 2018 / Accepted: 31 January 2019
© Springer Science+Business Media, LLC, part of Springer Nature 2019

Abstract

Methane dehydroaromatization was studied over a series of K, Rh and Fe promoted 10 wt% Mo/HZSM-5 catalysts with different promoter loadings of 0.5, 1 and 1.5 wt% at 750 °C in a recirculating batch reactor. All the catalysts were reduced in H₂ at 750 °C prior to methane activation. K, Rh and Fe- promoted Mo/HZSM-5 catalysts were prepared by sequential impregnation. *N*-propylamine-temperature programmed desorption confirmed the significant modification in the acidity of the catalyst upon addition of K. Compared to 10 wt% Mo/HZSM-5, the conversion of CH₄ remained nearly unchanged for 1 wt% K-promoted catalyst but decreased by ~46% for 1 wt% Rh promoted catalyst and by ~4.3% for Fe-promoted catalyst after 255 min of reaction. The conversion of CH₄ further decreased with increase in K and Rh loading but increased with increase in Fe loading. Compared to Rh and Fe-promoted catalysts, K-promoted catalyst exhibited better selectivity for C₆H₆ after 255 min of reaction. The temperature programmed oxidation results revealed that K promoted catalyst significantly reduced coking. 1 wt% K added to 10 wt% Mo/HZSM-5 exhibited optimum performance, where the conversion of CH₄ was ~28%, selectivity of C₆H₆ was ~50% while the selectivity of carbon was ~47% after 255 min of reaction.

Graphical Abstract



Keywords Methane dehydroaromatization · Promoters · K-Mo/HZSM-5 · H₂ pretreatment · β -Mo₂C

✉ Hema Ramsurn
hema-ramsurn@utulsa.edu

¹ Russell School of Chemical Engineering, The University of Tulsa, 800 South Tucker Drive, Tulsa, OK 74104, USA

1 Introduction

The low cost of natural gas has created an interest in its conversion to high value chemicals and fuels. The major component of natural gas is methane which generally consists of about 70–90% by volume of the total. This methane can be converted into valuable chemicals by both direct and indirect routes. The indirect conversion of methane by Fisher-Tropsch to methanol followed by methanol-to-gasoline is currently a more commercially viable process than the direct conversion of methane to aromatics and has been practiced on large scales for decades [1, 2]. Direct methane conversion technologies include oxidative coupling of methane, partial oxidation of methane and methane dehydroaromatization (MDA). These processes have barriers to commercialization including limited conversions, poor selectivity to desired products and catalyst deactivation. Direct conversion of methane to aromatics under non-oxidative conditions was first studied by Wang et al. [3] in 1993. MDA effectively occurs over a transition-metal incorporated in a bifunctional zeolite catalyst. Past studies investigated various metals which include Mo [4], Zn [5], W [6, 7], Re [8] and Ga [9] over HZSM-5. MDA was also studied over Mo supported on different zeolites like HSAPO-34 [10], HY [10], HZSM-5 [11], HMCM-36 [12] and HMCM-49 [13]. The most active catalysts were found to be molybdenum loaded on HZSM-5 [4] and HMCM-22 [14] with high selectivity of 50–80% for benzene. Though Mo/HZSM-5 was found to be a promising catalyst for MDA, the significant amount of coke formation during the MDA reaction rapidly deactivates the catalyst thus affecting the stability of the catalyst and selectivity of desired aromatics. To overcome catalyst coking and to improve the selectivity of desired hydrocarbons, several techniques have been investigated including structural modification of the surface of zeolite support [15–17], use of composite catalyst (Mo/HZSM-5 along with Gd doped CeO₂) [18], addition of gases like H₂, H₂O [19], CO [20], CO₂ [21, 22] during the CH₄ activation, modifying the pretreatment conditions of the catalyst [23], addition of promoters [24] and periodic switching between CH₄ and H₂ during the MDA reaction [25]. In literature, it has been suggested that addition of a second metal to Mo/HZSM-5 as a promotor can suppress the coke formation and enhance the aromatic yield [26]. Among the transition metals, Fe [27, 28] and Zn [29] are the most commonly used promoters for Mo/HZSM-5. Apart from these metals, other metals like Ga [30], Sn [31], Mg [32], Ru [33, 34], Li [4] were also used as promoters for Mo/HZSM-5 to enhance the MDA reaction. Xu et al. [35] studied the effects of transition metal promoted Mo/HZSM-5 prepared by co-impregnation on MDA at 800 °C in

periodic CH₄–H₂ switch mode. It was found that promoting metals like Fe, Co, Ru and Pd enhanced the CH₄ conversion, while metals like Cu and Zn had insignificant improvement on CH₄ conversion and metals like Cr and Mn decreased the catalyst's activity. Their studies claimed that the promotional effect of Fe is due to the formation of Fe induced carbon nanotubes. During the H₂ flow mode, the presence of Fe enhanced the surface coke removal resulting in better stability of the catalyst [27]. The same study also concluded that the size of zeolite support is significantly important during the catalytic activity. Fe promoted 5% Mo/HZSM-5 (different Fe loadings of 0.3, 0.5, 1 and 2%) based on nanosized zeolites improved the activity and stability of the catalyst while the Fe promoted 5% Mo/HZSM-5 based on micro-sized zeolites had negligible promotional effect. The improved activity and stability of the nanosized zeolites were due to the disagglomeration of the micro-sized crystals caused by the growth of Fe induced carbon nanotubes. Though the activity of the catalyst was enhanced, the selectivity of benzene was lower in Fe promoted 5% Mo/HZSM-5 on both nanosized and micro-sized zeolites, compared to the unmodified 5% Mo/HZSM-5 [36]. Sun et al. [37, 38] doped the Mo/HZSM-5 with nanosized Fe by mechanical ball milling and investigated its effect on MDA and reported an increase in methane conversion upon addition of nanosized Fe particles. Abdelsayed et al. [39] studied the promotional effect of Fe and Zn on Mo/HZSM-5 and reported that when Fe (0.3%) was used as a promotor, the benzene formation rate was increased by 35% while the Zn (1%) promoted catalyst showed a 10% increase in benzene formation rate. However, using both Zn (1%) and Fe (0.3%) simultaneously as promoters, reduced the benzene formation by 31%. Aboul-Gheit et al. [29, 40] replaced half the Mo concentration in the catalyst with Zn in 6% Mo/HZSM-5 and noticed an enhancement in benzene selectivity. Their results claimed that promoters with higher electronegativity decreased the selectivity of benzene and naphthalene. Their work also included the investigation of oxygen free natural gas conversion over 6% Mo/HZSM-5 and 3% Fe, 3% Co and 3% Ni substituted 3% Mo/HZSM-5 prepared by mechanical mixing. Results revealed that 6% Mo/HZSM-5 exhibited better aromatization activity when compared to group VIII metals promoted Mo/HZSM-5. Zeng et al. [7] studied the promotional effect of Zn over W/HZSM-5 and Mo/HZSM-5 prepared in the pH range of 2–3 stabilized by H₂SO₄ and reported that addition of Zn (1.5%) improved the catalyst activity and selectivity of benzene in both Mo and W/HZSM-5 at 800 °C. Similarly, Xiong et al. [6, 41] studied the effect of adding Zn (1.5%) on W/HZSM-5 and reported an increase in catalyst activity and benzene selectivity. Tshabalala et al. [31, 42] investigated the effect of adding Pt and Sn to Mo/HZSM-5. Addition of Pt (0.5%)

increased the methane conversion and aromatic selectivity while increase in tin (0.05–0.2%) loading decreased the methane conversion but increased the selectivity of aromatics. Their studies also revealed that the effect of preparation method highly influenced the aromatic and coke selectivity and sequential impregnation of Sn followed by Pt over Mo/HZSM-5 exhibited high benzene selectivity and low carbon deposits. Similarly, Tan et al. [43] claimed that Pt-Mo/HZSM-5 prepared by impregnating Pt (0.3%) on Mo/HZSM-5 showed better activity than Pt-Mo/HZSM-5 prepared by impregnating HZSM-5 with a mixture of Pt and Mo precursors. Effects of addition of Ga to Mo/HZSM-5 was studied by Liu et al. [30, 44] and their results concluded that adding Ga (0.1–1%) improved the performance of the catalyst, increased the yields of C₂–C₁₁ hydrocarbons and decreased the coke. It was also observed that Ga helps in effective adsorption of CO₂ and CO while improving alkene formation. Shu et al. [45] reported an enhancement in catalytic activity for a 2 wt% Mo/HZSM-5 incorporated with Ru with a Mo/Ru ratio between 0.3 and 0.7. Addition of Ru decreased the acidic sites in the zeolite and promoted the reduction of Mo species. Martínez and Peris [46] studied the effect of replacing the acidic protons in the zeolite with alkali and alkaline-earth cations. Compared to Mo/HZSM-5, Mo loaded on alkali (Na⁺ and Cs⁺) and alkaline (Ca²⁺ and Mg²⁺) ions modified zeolite exhibited less catalytic activity and enhanced benzene selectivity. In contrary, Cheng et al. [32] reported that Mg (1%) promoted Mo/HZSM-5 prepared by impregnation method improved both the activity of the catalyst and the selectivity of benzene. Wang et al. [47] compared the promotional effects of W (0.5%), V (1%) and Zr (0.5–2%) over Mo/HZSM-5 at 650 °C and reported that addition of W and Zr increased the catalyst activity and benzene selectivity while addition of V decreased the activity and benzene selectivity. Kojima et al. [48] examined the effects of adding noble metals like Pt and Rh (molar ratio of noble metal/Mo = 0.2) on Mo/HZSM-5 and Mo/HMCM-22 by co-impregnation and reported that these noble metals suppressed coke formation on the Bronsted acid sites. Moreover, in the presence of Pt and Rh, α-MoC_{1-x} was formed as the active site instead of Mo₂C. Though significant research has been done on the addition of the promoting metals Fe and Zn to zeolite supported Mo catalyst, results based on addition of an alkali metal like K and noble metal like Rh are scantily reported in literature. Thus, this work primarily focuses on studying the individual promotional effects of K and Rh added to Mo/HZSM-5 along with Fe (well-known promoter) on MDA at 750 °C and 1 atm using hydrogen as the reduction medium for the catalyst in a recirculating batch reactor.

2 Experimental

2.1 Catalyst Preparation

ZSM-5 (SiO₂/Al₂O₃ = 30) from zeolyst international was used as a standard support for preparing all the catalysts. Mo/HZSM-5 was synthesized by incipient wetness impregnation. Required amount of (NH₄)₆Mo₇O₂₄·4H₂O (Ammonium Hepta Molybdate, AHM) salt (equivalent to 10 wt% Mo/HZSM-5) was dissolved in a known amount of deionized water sufficiently enough to completely wet the zeolite support and this aqueous AHM solution was added drop by drop to the zeolite support. The resulting mixture was dried at 120 °C for 5 h and calcined at 500 °C in air for 5 h. A series of K, Rh and Fe promoted Mo/HZSM-5 catalysts were prepared by sequential impregnation method. K₂CO₃·1.5H₂O, RhCl₃·3H₂O and Fe(NO₃)₂·9H₂O were used as the precursors for K, Rh and Fe promoters respectively. In this case, Mo/HZSM-5 was first prepared by following the above-mentioned procedure. After calcining the catalyst at 500 °C it was cooled to room temperature and then it was impregnated with the corresponding promoting metal salt solution and finally the resulting mixture was dried at 120 °C for 5 h and calcined at 500 °C in air for 5 h. Finally, the catalysts were pressed and sieved to particle size in the range of 20–40 mesh. The prepared catalysts were denoted as x P-10 Mo/HZSM-5 where x corresponds to the weight percent (0.5, 1, 1.5 wt%) of the promoter (P).

2.2 Catalytic Reaction System

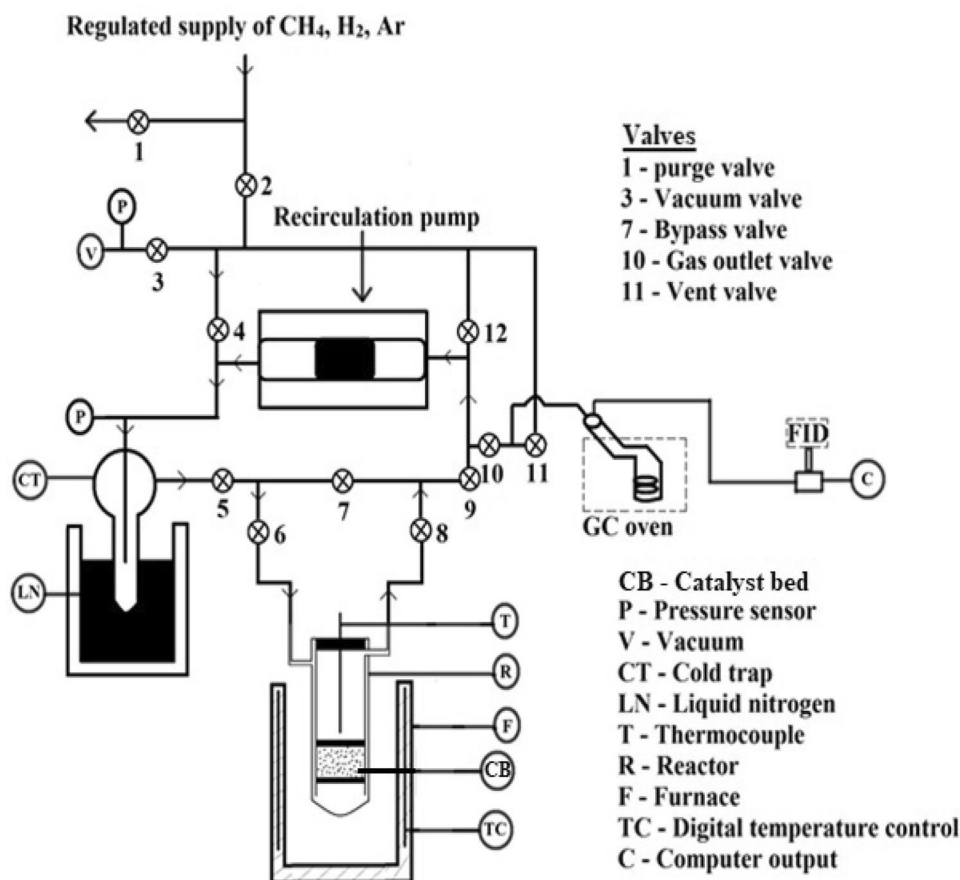
The schematic representation of the batch circulation reactor system is shown in Fig. 1. The working principle of the reactor system, catalytic reduction and reaction procedure and material balance considerations were explained in detail in our previous work [49]. All the catalytic reaction experiments were carried out at 750 °C and the reaction products were analyzed using 5880 HP GC-FID. The amount of carbon which is not detected by the GC-FID is also included in the carbon balance, considering the missing carbon as “carbon” (carbon with molecular weight of 12) which includes the carbon consumed for active site formation, dissociation of CH₄ into CH_x species and the coke formed by agglomeration of heavier aromatics [30].

The conversion of methane is given by:

Conversion of methane (%) = $\frac{N_0 - N_t}{N_0} \times 100$ where N₀ is the initial moles of methane and N_t is the moles of methane available at time t.

The selectivity of benzene is given by:

Fig. 1 Schematic diagram of catalytic reactor system



Selectivity of Benzene (%) = $\frac{N(B)_t}{N(M)_t} \times 100$ where $N(B)_t$ is the total moles benzene formed at time t and $N(M)_t$ is the total moles of methane converted at time t .

2.3 Catalyst Characterization

2.3.1 Brunauer–Emmett–Teller Surface Area

The surface area of the prepared catalysts was measured by BET method using nitrogen as adsorbate on a Quantachrome autosorb one unit. The degassing temperature was 300 °C for 24 h and isotherms were measured at −196 °C.

2.3.2 Inductively Coupled Plasma–Optical Emission Spectrometry (ICP–OES)

Agilent 5110 ICP–OES was used to quantify the elements present in the catalyst. Acid digestion of the catalyst was performed to prepare sample solution for the analysis. Approximately 100 mg of catalyst was taken in a digestion vessel and trace metal grade HNO₃ (4 ml), HCl (4 ml) and HF (2 ml) were added. The mixture in the vessel was heated to 180 °C at a rate of 10 °C/min and held at 180 °C for

15 min. Once a clear solution was obtained, the samples were diluted before analyzing in ICP–OES.

2.3.3 Scanning Electron Microscopy (SEM)

FEI Inspect 60 scanning electron microscope was used to study the surface morphology of the catalyst samples.

2.3.4 X-ray Diffraction (XRD)

Rigaku miniflex 600 diffractometer with PDXL software was used to obtain X-ray diffraction patterns and perform data analysis. The X-ray source was operated at 40 kW and 15 mA (600 Watts) with Cu Kα-1 X-rays. The diffractometer was equipped with a monochromator to reduce iron fluorescence. The samples were analyzed in the range of $2\theta = 10\text{--}80^\circ$ by $0.04^\circ/\text{step}$ with a count time of 2 s per step.

2.3.5 n-Propylamine–Temperature Programmed Desorption (NPA–TPD)

NPA–TPD measurements were performed on Mo loaded on HZSM-5 catalysts using a thermogravimetric analyzer (Perkin-Elmer Pyris-1 TGA). The results will help in

understanding the effect of Mo addition on acidic properties of the zeolite support. Approximately 20 mg of the dry sample was placed in a Pt sample pan in the TGA and the weight was recorded. The sample was dried at 350 °C in He and cooled to 50 °C before treatment in 20% H₂/80% He by heating to 750 °C to match the experimental condition. The sample was then cooled to 50 °C before exposure to NPA. Once the sample attained a constant weight, NPA supply was stopped and the sample was purged with He for 10 min. Finally, the sample was heated to 550 °C at a rate of 5 °C/min in He and weight loss due to the desorption of NPA was recorded as the function of temperature.

2.3.6 Temperature Programmed Reduction (TPR)

Catalyst reduction conditions were established by performing TPR experiments using thermogravimetric analyzer (Perkin-Elmer Pyris-1 TGA). To dry the sample, approximately 20 mg of sample was placed in a Pt sample pan in the TGA and heated to 350 °C in He atmosphere. Later the sample was cooled to 50 °C and the weight was recorded. TPR was performed in a 20% H₂/80% He atmosphere by heating from 50 to 750 °C and the corresponding weight loss was recorded. The temperature range where reduction took place was used to plan the catalyst reduction procedure for catalytic reaction studies.

2.3.7 Temperature Programmed Oxidation (TPO)

Carbon deposits in the spent catalysts were quantified by TPO measurements using thermogravimetric analyzer (Perkin-Elmer Pyris-1 TGA). To dry the spent catalyst, approximately 20 mg was placed in a Pt sample pan in the TGA and heated to 350 °C in He atmosphere. Once the drying was complete, the sample was cooled to 50 °C and the weight was recorded. Finally, in a 20% O₂/80% He atmosphere, the dried sample was heated from 50 to 750 °C and the corresponding weight loss was recorded.

2.3.8 CO-Chemisorption Studies

The CO-chemisorption studies were performed in a volumetric adsorption system. Approximately 500 g of sample was dried under vacuum at 350 °C. The sample was then reduced in H₂ at 600 °C for 90 min and at 750 °C for 30 min to match the experimental pretreatment conditions. Later, the system was evacuated to remove the H₂ and the sample was cooled to room temperature. A water bath was used as a thermostat during the CO chemisorption. Volumetric measurements were used to determine the amount of CO chemisorbed in a conventional volumetric adsorption device. The CO uptake was taken as the difference between the total amount adsorbed at room temperature and the amount of

weakly adsorbed material. Weakly adsorbed material was determined by evacuating a fully covered material and measuring the uptake again at room temperature.

3 Result and Discussion

3.1 Catalyst Characterization

3.1.1 Surface Area

Table 1 shows the results of BET surface area and the pore volume of the pure HZSM-5 compared with Mo/HZSM-5 and K, Rh and Fe-promoted Mo/HZSM-5 catalysts. The surface area and the pore volume of Mo/HZSM-5 decreased when compared to HZSM-5. High dispersion of Mo species on the surface of HZSM-5 could possibly be the cause for significant decrease in the surface area (Sect. 3.1.6). Surface area and pore volume of promoted Mo/HZSM-5 shows that addition of a promoter metal had affected the dispersion of Mo species to some extent as the surface areas of K, Rh and Fe-promoted catalysts were slightly higher than that of Mo/HZSM-5. The increase in surface area of the catalyst upon addition of Fe is in accordance with the findings Xu et al. [36]. From Table 1, it is evident that impregnating metal species on ZSM-5 did not significantly affect the pore volume and average pore size (D) of the catalyst. Thus, addition of Mo species and other promoter metals has no serious effect on the pore structure of the zeolite.

3.1.2 Inductively Coupled Plasma-Optical Emission Spectroscopy (ICP-OES)

Table 2 compares the expected and actual metal loadings in the catalysts analyzed using the ICP-OES. In the sequential impregnation method where molybdenum was loaded first followed by the promoter metal, the catalysts were calcined twice. Thus, during the second stage calcination, sublimation of Mo species in air around 500 °C is possible. This accounts for loss of Mo and the actual Mo loading was less compared to the expected Mo loading.

Table 1 Physical properties of HZSM-5 based catalysts

Catalyst	Surface area (m ² /g)	Pore volume (cm ³ /g)	Avg pore size (D) (Å)
HZSM-5	353	0.16	30.69
10 Mo/HZSM-5	237	0.15	30.62
1.5 K-10 Mo/HZSM-5	243	0.13	30.60
1.5 Rh-10 Mo/HZSM-5	247	0.13	30.56
1.5 Fe-10 Mo/HZSM-5	266	0.15	30.58

Table 2 Quantitative analysis of elements in the catalysts

Sample	Expected wt%				Actual wt%			
	Mo	K	Rh	Fe	Mo	K	Rh	Fe
10 Mo/HZSM-5	10	–	–	–	8.9	–	–	–
1.5 K–10 Mo/HZSM-5	10	1.5	–	–	8.6	1.3	–	–
1.5 Rh–10 Mo/HZSM-5	10	–	1.5	–	8.9	–	1.5	–
1.5 Fe–10 Mo/HZSM-5	10	–	–	1.5	9.5	–	–	1.6

3.1.3 X-ray Diffraction (XRD) Analysis

The crystallinity of K, Rh and Fe-promoted Mo/HZSM-5 catalysts was investigated by X-ray diffraction analysis. Figure 2a shows the XRD patterns of the freshly prepared catalysts calcined at 500 °C in air. Peaks at $2\theta = 12.9^\circ$, 27.4° corresponding to the α -MoO₃ orthorhombic phase are apparent in all the catalysts. In case of K promoted Mo/HZSM-5 catalysts, increase in K loading didn't significantly affect the intensity of MoO₃ species. But in case of Rh and Fe promoted catalysts with increase in Rh and Fe loadings, the intensity of MoO₃ decreases. Thus, the dispersion of MoO₃ on the zeolite has been modified with the addition of Fe and Rh species. Figure 2b shows the XRD peak of 10 wt% Mo/HZSM-5 catalyst reduced in H₂ at 750 °C. The diffraction peak at 2θ value of 40.51° corresponds to elemental molybdenum phase. Thus, it was evident that the MoO₃ species were reduced to metallic Mo during the H₂ reduction.

3.1.4 Temperature Programmed Reduction (TPR)

TPR is the most appropriate method to study the metal support interaction in terms of metal reduction as a function of temperature. Figure 3 shows the weight changes of the catalysts during microbalance reduction. Before reduction, the catalyst samples were dried in the microbalance at about 350 °C in He. In case of Mo/HZSM-5 (Fig. 3, (5)), the first reduction peak was observed at around 550 °C which corresponds to the reduction of MoO₃ species to MoO₂ species and the second reduction peak was observed at around 715 °C which corresponds to the reduction of MoO₂ to Mo species which is in accordance with the findings of Tshabalala et al. [42]. The K and Fe-promoted Mo/HZSM-5 catalysts (Fig. 3, (6), (8)) exhibited similar reduction trends for Mo species where reduction of MoO₃ to MoO₂ occurred between 550 and 575 °C and reduction of MoO₂ to Mo occurred between 720 and 750 °C. In case of Rh–Mo/HZSM-5 (Fig. 3, (7)) the first reduction peak was observed in the range of 400–550 °C and the second reduction peak was observed around 750 °C. On a quantitative basis, for a 10 wt% Mo/HZSM-5 catalyst, the expected relative weight loss (TA curve in Fig. 3) after the reduction of MoO₃ to Mo is ~5%. The experimental weight loss for 10 wt% Mo/HZSM-5, K and Fe-promoted 10 wt% Mo/HZSM-5 (Fig. 3,

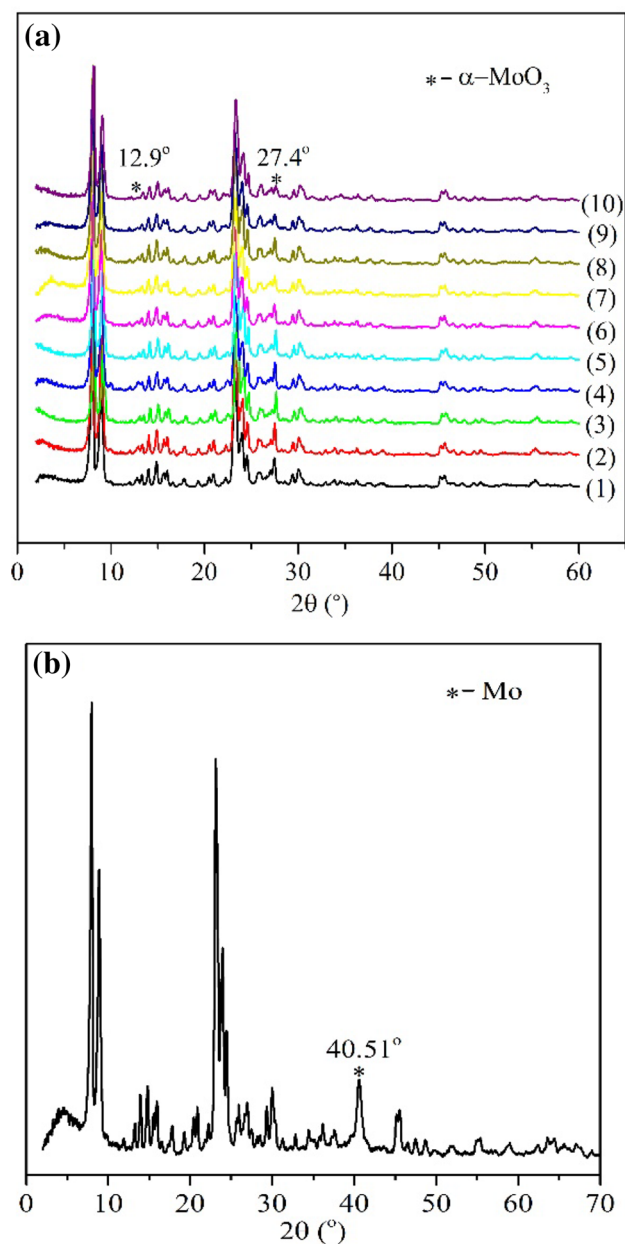


Fig. 2 XRD patterns of **a** fresh catalyst (1) 10 wt% Mo/HZMS-5 (2) 0.5 K–10 Mo/HZSM-5 (3) 1 K–10 Mo/HZSM-5 (4) 1.5 K–10 Mo/HZSM-5 (5) 0.5 Rh–10 Mo/HZSM-5 (6) 1 Rh–10 Mo/HZSM-5 (7) 1.5 Rh–10 Mo/HZSM-5 (8) 0.5 Fe–10 Mo/HZSM-5 (9) 1 Fe–10 Mo/HZSM-5 (10) 1.5 Fe–10 Mo/HZSM-5 and **b** 10 wt% Mo/HZSM-5 reduced catalyst

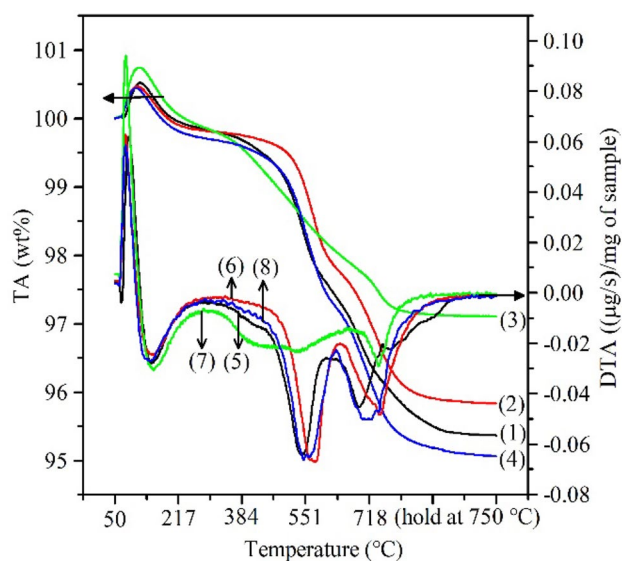


Fig. 3 TPR profiles of 10 wt% Mo/HZSM-5 [(1) TA, (5) DTA], 1.5 K-10 Mo/HZSM-5 [(2) TA, (6) DTA], 1.5 Rh-10 Mo/HZSM-5 [(3) TA, (7) DTA] and 1.5 Fe-10 Mo/HZSM-5 [(4) TA, (8) DTA]

(1), (2), and (4)) catalysts were 4.64%, 4.18% and 4.95% which were equivalent to ~9.37%, ~8.44%, ~10% of Mo loading respectively. These results were consistent with the results of ICP-OES analysis (Sect. 3.1.2). For Rh-promoted Mo/HZSM-5 catalyst, the weight loss shown in the TA curve (Fig. 3, (3)) was only 2.9% which is equivalent to 5.85% of Mo loading, whereas the ICP-OES result reported 8.9% of Mo. This implies that not all the MoO₃ species were reduced to Mo. It can be postulated that either a portion of Mo species has been covered by the Rh species or agglomeration of MoO₃ species occurred in the presence of Rh and hindered the completed reduction of all the Mo species on the catalyst as discussed in Sect. 3.1.6. Only the portion of MoO₃ reduced to MoO₂, were further reduced to Mo at around 750 °C as shown by two distinct peaks in the DTA curve of Rh-promoted catalyst (Fig. 3, (7)).

3.1.5 *N*-propyl Amine-Temperature Programmed Desorption (NPA-TPD)

Mo/HZSM-5 acts as a bifunctional catalyst where the Bronsted acid (H⁺) sites in the zeolite plays a crucial role in MDA reaction. To assess the effect on acidic properties of HZSM-5 on addition of metals, NPA-TPD studies were performed. Figure 4 shows the TA (Thermal analysis) and the corresponding, DTA (derivative) curves for catalysts subjected to NPA-TPD studies. The TA (Fig. 4, (1)) and DTA (Fig. 4, (6)) curves for pure HZSM-5 were similar to the results reported by Price et al. [50–52], where the intensity of the observed bands depends on the nature and density of the acid sites in the zeolite. The “plateau region”

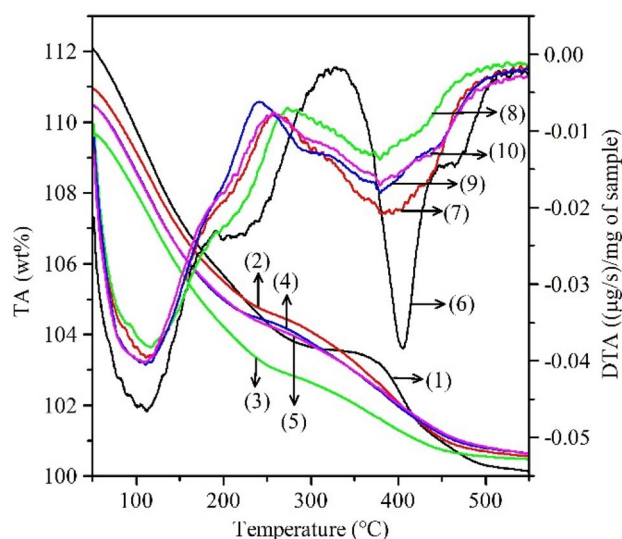


Fig. 4 NPA-TPD profiles of pure HZSM-5 [(1) TA, (6) DTA], 10 wt% Mo/HZSM-5 [(2) TA, (7) DTA], 1.5 K-10 Mo/HZSM-5 [(3) TA, (8) DTA], 1.5 Rh-10 Mo/HZSM-5 [(4) TA, (9) DTA] and 1.5 Fe-10 Mo/HZSM-5 [(5) TA, (10) DTA]

in the TA curve of HZSM-5, which is in the temperature range 300–350 °C, is characteristic of weakly bound NPA having been desorbed and only a 1/1 NPA to H⁺ adsorbed species (an *n*-propylammonium cation) remains. Desorption of the amine from these sites results in a band observed at about 400 °C [50]. In the TA (Fig. 4, (2)) and DTA (Fig. 4, (7)) spectra of Mo/HZSM-5 catalysts, the plateau region is difficult to observe as the plateau and the band at 400 °C have shifted when compared to the pure HZSM-5. Moreover, addition of promoters further modified the plateau region and the intensity of the band at 400 °C. Rh (Fig. 4, (4) and (9)) and Fe (Fig. 4, (5) and (10)) -promoted Mo/HZSM-5 catalysts showed similar trends on NPA desorption but addition of K (Fig. 4, (3), (8)) to Mo/HZSM-5 exhibited significant changes in plateau region and the band at 400 °C. The adsorbed NPA species on HZSM-5 almost completely desorbed at the end of the experiment. From Fig. 4, the TA curve (1) reached close to 100 wt%, which is the initial weight of the sample after drying. However, each spectra of the promoted catalyst showed a significant remnant of undesorbed material at 520 °C at the end of the experiment,

Table 3 CO uptake by Mo/HZSM-5 and promoted Mo/HMZS-5

Catalyst	CO uptake (μmol/g)
10 Mo/HZSM-5	287.08
1.5 K-10 Mo/HZSM-5	159.59
1.5 Rh-10 Mo/HZSM-5	62.52
1.5 Fe-10 Mo/HZSM-5	212.36

Fig. 5 Conversion of CH_4 at 750 °C over 10 wt% Mo/HZSM-5 compared with promoted 10 wt% Mo/HZSM-5 with different promoter loadings of **a** 0.5 wt%, **b** 1 wt%, **c** 1.5 wt%

indicative of a carbonaceous residue likely from metal catalyzed polymerization of NPA as previously reported by Price et al. [51]. This indicates that the metal species have migrated into the zeolite lattice and modified the acidity of the zeolite.

3.1.6 CO-chemisorption Studies

Table 3 shows the amount of CO chemisorbed by Mo/HZSM-5 and metal promoted Mo/HZSM-5 catalysts at room temperature. For Mo/HZSM-5, the CO uptake was 287.08 $\mu\text{mol/g}$ and the metal dispersion (the fraction of Mo atoms on the surface of the Mo crystallites) was 0.55, assuming dissociative adsorption [53] (one CO per two Mo atoms at room temperature). In case of promoted Mo/HZSM-5 materials, though the Mo loading remains the same, the CO uptake is reduced, especially for Rh–Mo/HZSM-5. This is possibly due to the decrease in the number of exposed Mo atoms as the sequentially added promoter might have covered a portion of the surface of the Mo species or due to the sintering and agglomeration of the Mo species (reduced Mo dispersion) during the second stage calcination. Also, in case of promoted Mo/HZSM-5 materials, since CO was adsorbed on both Mo and the promoted metal species, the calculation of actual Mo dispersion is not possible.

4 Catalytic Results

4.1 Effect of Adding K, Rh and Fe as Promoters on Mo/HZSM-5

4.1.1 Conversion of CH_4 on Promoted Mo/HZSM-5 Catalyst at 750 °C

The effect of adding promoters (K, Rh and Fe) with different loadings of 0.5 wt%, 1 wt% and 1.5 wt% over 10 wt% Mo/HZSM-5 on methane aromatization was studied in detail. Figure 5 shows the conversion of CH_4 on promoted Mo/HZSM-5 catalyst compared with the 10 wt% Mo/HZSM-5 at 750 °C. When compared to the 10 wt% Mo/HZSM-5, addition of 0.5 wt% promoter (Fig. 5a) exhibited an improved conversion in case of K-promoted catalyst. For the 0.5 wt% K-promoted catalyst, the conversion of CH_4 was ~16.5% and ~32% at the 10 and 255 min reaction time, respectively. This corresponds to an increase of ~13.5% and ~16.5% when compared to 10 wt% Mo/HZSM-5 for the same reaction times. For 0.5 wt% Fe-promoted catalyst, the conversion of CH_4 was ~16% and ~5.8% less than that of 10 wt%

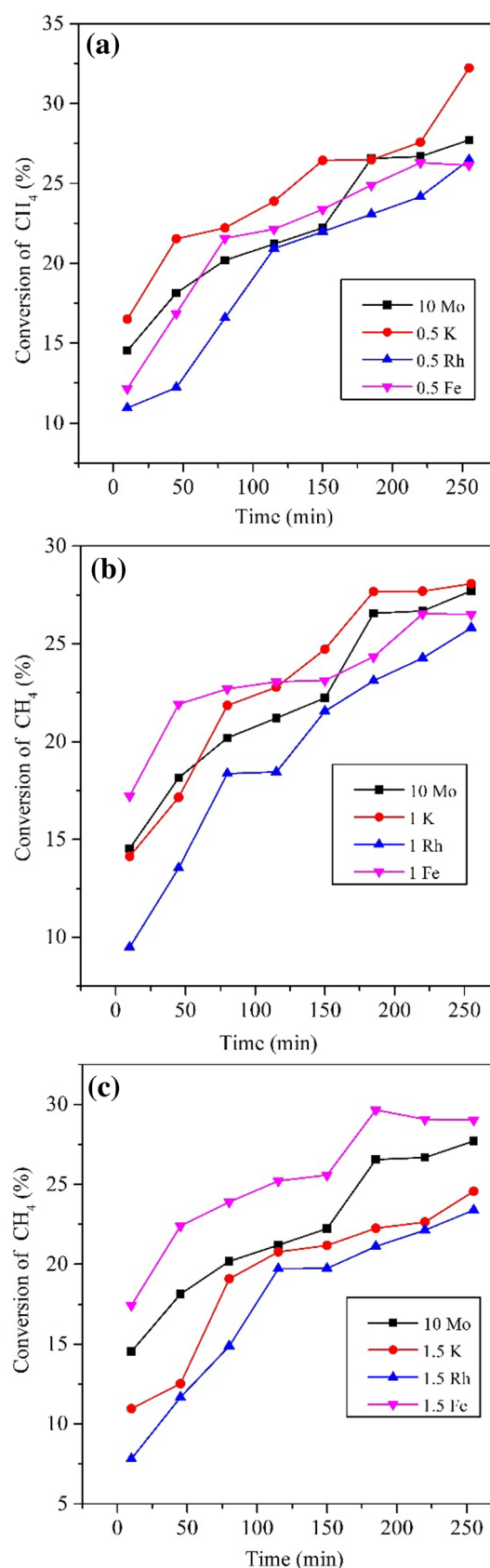


Fig. 6 Selectivity of C_6H_6 at 750 °C over 10 wt% Mo/HZSM-5 compared with promoted 10 wt% Mo/HZSM-5 with different promoter loadings of **a** 0.5 wt%, **b** 1 wt%, **c** 1.5 wt%

Mo/HZSM-5 at 10 and 255 min of reaction time respectively. The Rh-promoted catalyst exhibited the least CH_4 conversion. The conversion at 10 and 255 min of reaction was 25% and ~5% less when compared to the 10 wt% Mo/HZSM-5. Increasing the promoter loading exhibited different trends for each promoter metal as shown in Fig. 5b, c. The conversion of CH_4 decreased with increasing loading of K and Rh. The conversion of CH_4 for 1 wt% K-promoted catalyst was almost similar to that of 10 wt% Mo/HZSM-5 but the conversion dropped by ~25% and ~12% at 10 min and 255 min of reaction when the K loading was increased to 1.5 wt%. Increasing the Rh loading to 1 wt% and 1.5 wt% decreased the conversion by ~35% and ~46% by ~6.8% and ~15.5%, at 10 and 255 min, respectively. Increasing the Fe loading to 1 wt% and 1.5 wt% improved the conversion of CH_4 at 10 min of reaction by 18.7% and 20.1% respectively. At 255 min, the conversion of CH_4 decreased by ~4.3% and increased by ~4.7% for 1 wt% and 1.5 wt%, respectively.

4.1.2 Selectivity of C_6H_6 , C_2 , and Carbon on Promoted Mo/HZSM-5 Catalyst at 750 °C

Figure 6 compares the selectivity of C_6H_6 on 10 wt% Mo/HZSM-5 and promoted 10 wt% Mo/HZSM-5 at 750 °C. The 10 wt% Mo/HZSM-5 exhibited the maximum selectivity of ~80% for C_6H_6 within the first 45 min of reaction but the selectivity of C_6H_6 decreased with increasing reaction time and at 255 min of reaction the selectivity of C_6H_6 was less than ~30%. In case of 0.5 wt% K-promoted catalysts, though the selectivity increased during the first 80 min of reaction and reached a maximum of ~60%, it gradually decreased to ~40% after 255 min of reaction. Rh exhibited the least selectivity for C_6H_6 during the first 10 min of reaction but the selectivity of C_6H_6 increased with increasing reaction time and was stable at ~40% after 255 min reaction. At 0.5 wt% promoter loading, the initial selectivity of C_6H_6 for Fe-promoted catalyst was ~70% but it steadily decreased with increasing reaction time and dropped to ~25% after 255 min of reaction. With increase in promoter loading, the selectivity of C_6H_6 increased in case of K-promoted catalyst. For 1 wt% and 1.5 wt% K loadings, the C_6H_6 selectivity reached a maximum of ~66% and ~76% and it was stable around ~50% and 60% respectively after 255 min of reaction. In case of Fe-promoted catalyst, the C_6H_6 selectivity decreased with increasing promoter loading. The C_6H_6 selectivity of 10 min and 255 min of reaction time was ~44% and 19% for 1 wt% Fe and ~33% and ~9% for 1.5 wt% Fe. 1 wt% and 1.5 wt% Rh showed trends similar to that of 0.5 wt% Rh where the initial C_6H_6 selectivity was least compared

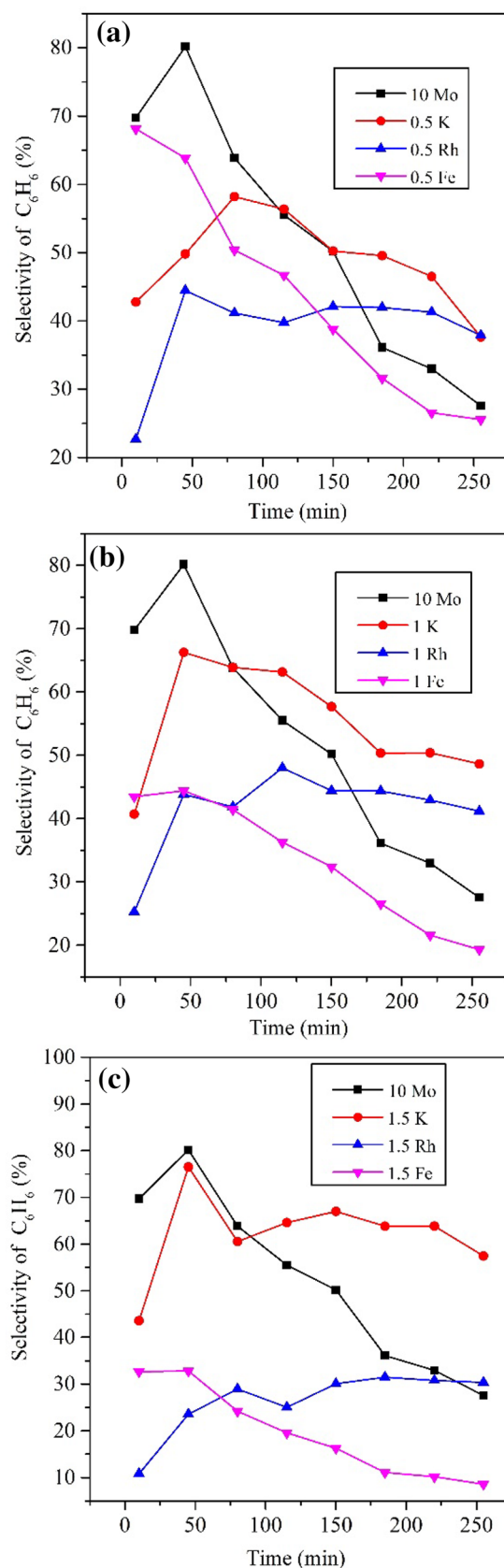


Fig. 7 Selectivity of C2 at 750 °C over 10 wt% Mo/HZSM-5 compared with promoted 10 wt% Mo/HZSM-5 with different promoter loadings of **a** 0.5 wt%, **b** 1 wt%, **c** 1.5 wt%

to the catalysts with same loadings of other promoters and the selectivity steadily increased and was stable around ~35–45% after 255 min of reaction. Thus, after 255 min of reaction, comparing all three promoters, K is the only promoter which on addition to Mo/HZSM-5 has improved the selectivity of C₆H₆.

Figure 7 compares the selectivity of C2 hydrocarbons on 10 wt% Mo/HZSM-5 and promoted 10 wt% Mo/HZSM-5 at 750 °C. In MDA studies, generally the selectivity of C2 hydrocarbons is significantly less when compared to the selectivity of aromatics. Thermodynamic limitations favor methane aromatization over methane dimerization at MDA reaction temperatures of around 700–750 °C. Methane dimerization is feasible at 1350 °C where the Gibbs free energy of the reaction is zero ($\Delta G_r = 0$) whereas methane aromatization is feasible at 1075 °C. ($\Delta G_r = 0$) [54, 55]. Compared to 10 wt% Mo/HZSM-5, the selectivity of C2 increased with the addition of K and Rh as promoters to Mo/HZSM-5 catalyst and decreased in the presence of Fe. With increase in K loading the selectivity of C2 increased. In case of Fe and Rh-promoted catalysts, the selectivity of C2 decreased with increase in promoter loading. Though the selectivity of C2 with respect to reaction time increased for Rh-promoted catalysts during the first 45 min of reaction, the selectivity of C2 decreased with increase in reaction time for all the catalysts.

Figure 8 compares the selectivity of carbon on 10 wt% Mo/HZSM-5 and promoted 10 wt% Mo/HZSM-5 at 750 °C. The carbon selectivity after 10 min of reaction was ~20% for 10 wt% Mo/HZSM-5 and it increased in the presence of a promoter. Since all the catalysts were reduced in H₂ at 750 °C, the K, Rh, Fe and Mo species were reduced to metallic state before introducing CH₄. Hence along with Mo, the promoter also activates CH₄. Thus, significant amounts of CH_x species are formed but dimerization of the activated methane species is possible only in the presence of active Mo₂C sites (Sect. 4.2). In case of Rh-promoted catalyst, the high selectivity of carbon after the first 10 min of reaction could possibly be because of the activation of CH₄ by Rh forming CH_x species. Furthermore, poor dispersion of Mo species in the presence of Rh (discussed in Sect. 3.1.4) decreased the CH₄ conversion (Sect. 4.1.1) and limited the availability of active sites for dimerization. Similarly, in case of Fe-promoted catalyst, though the conversion of CH₄ increased with increase in Fe loading (Sect. 4.1.1), possibly due to the activation of CH₄ by both Fe and Mo, the carbon selectivity increased with increase in both Fe loading and reaction time. After 255 min of reaction, Fe-promoted catalysts exhibited the maximum carbon selectivity. This is

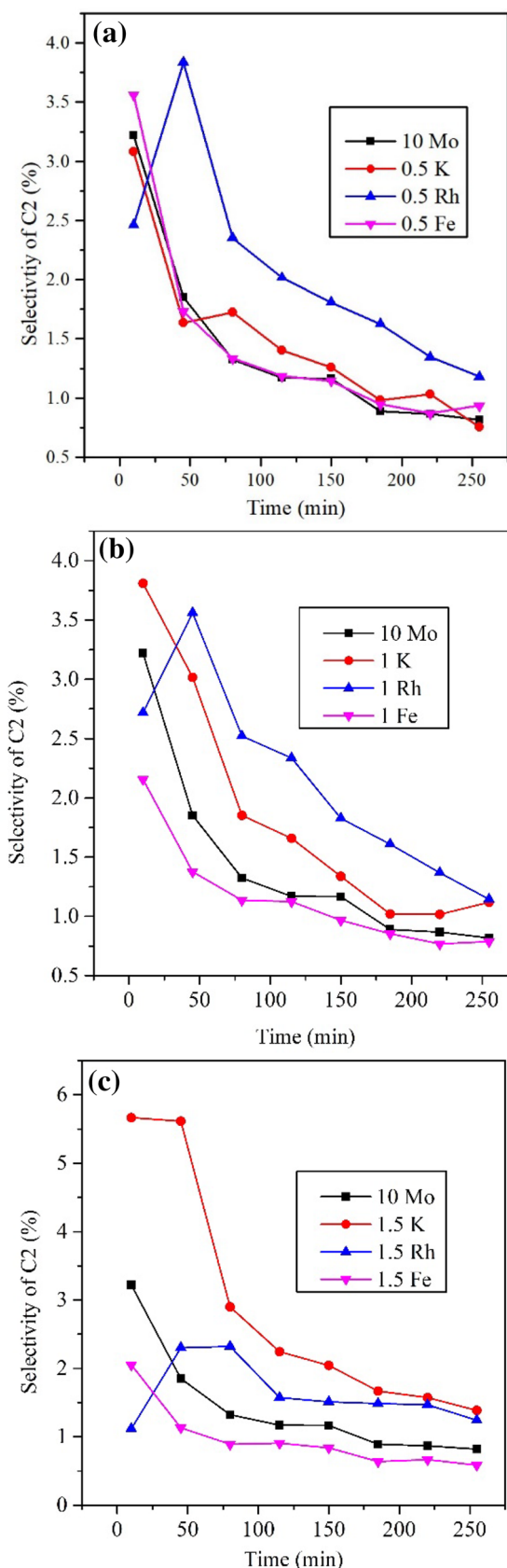
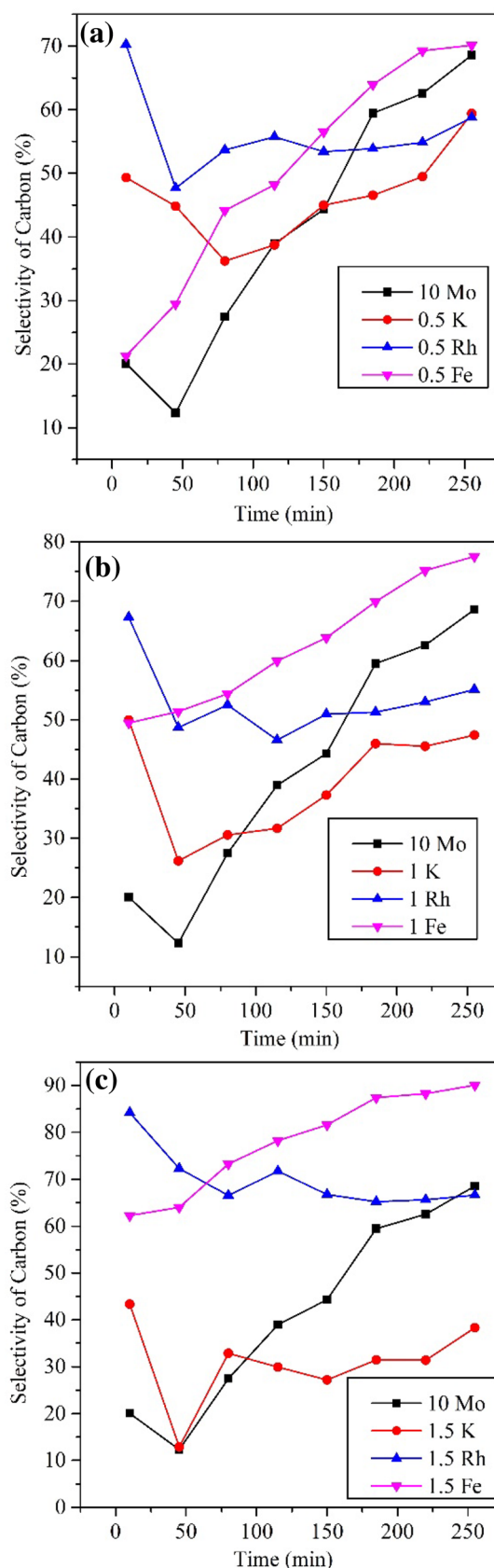


Fig. 8 Selectivity of carbon at 750 °C over 10 wt% Mo/HZSM-5 compared with promoted 10 wt% Mo/HZSM-5 with different promoter loadings of **a** 0.5 wt%, **b** 1 wt%, **c** 1.5 wt%

also in accordance with the TPO analysis of spent catalysts (Sect. 4.4). The SEM analysis of spent catalysts (Sect. 4.3) showed the presence of carbon nanostructures in the Fe-promoted catalyst, explaining the high carbon selectivity for Fe. The decrease in selectivity of C_6H_6 along with the formation of carbon nanostructures suggest that the presence of Fe increases the formation of carbon species at the expense of desired aromatic species [36]. In case of 10 wt% Mo/HZSM-5, K and Rh-promoted catalysts, the carbon selectivity initially decreased with increase in reaction time and then it increased. This increase is due to the coke formed through agglomeration of heavier hydrocarbons like C_6H_6 . In contrary to Rh and Fe-promoted catalysts, for K-promoted catalyst, the selectivity of carbon decreased with increasing K loading. 1.5 wt% K-promoted catalyst exhibited the lowest carbon selectivity of ~38% after 255 min of reaction which is ~54% less than the 10 wt% Mo/HZSM-5. Thus, K as a promoter inhibits the coke formation due to agglomeration of heavier hydrocarbons. It can be postulated that addition of K has significantly modified the acidity of the zeolite (Sect. 3.1.5) where availability of H^+ sites for agglomeration of hydrocarbons to form coke is limited.

4.2 Active Species for MDA Reaction

Samples of all the spent catalysts were subjected to XRD analysis to study the active phases available for MDA reaction. From Fig. 9, it is evident that all the samples show sharp peaks at 2θ values equal to 34.5° , 37.9° , 39.4° , 52° which corresponds to β - Mo_2C [56]. Mo_2C is the only active phase present in all the catalysts. This is in contrast to the results of Kojima et al. [48] who stated that addition of a noble metal like Rh formed α - MoC_{1-x} phase as an active site. The catalyst pretreatment condition significantly influences the formation of active sites. Kojima et al. [48] pretreated Rh promoted catalysts in a mixture of CH_4 and H_2 . Under this pretreatment condition, Rh was reduced to its metallic state before the reduction of MoO_3 to MoO_2 and this metallic Rh acted as a catalyst to activate methane and formed $MoO_xH_yC_z$ (precursor for α - MoC_{1-x}). Based on our previous study [49] and in this work, all the catalysts were reduced to metallic state by H_2 before introducing CH_4 to reduce the induction time on C_6H_6 formation. Thus, for all catalysts, including the Rh-promoted catalyst, Mo_2C was formed as the active phase.



4.3 Scanning Electron Microscope (SEM) Analysis

Figure 10 shows the SEM images of all the spent catalysts. In case of 10 wt% Mo/HZSM-5, K and Rh-promoted catalysts there is no significant morphological difference in the surface of the spent catalyst. In case of Rh and K promoted Mo/HZSM-5, with increase in promotor loading, the particles tend to agglomerate on the catalyst surface (Fig. 10d and Fig. 10g). This agglomeration of metal species leads to decrease in the dispersion of active sites (Mo_2C sites) and could possibly be the cause for decrease in catalyst activity for CH_4 conversion as discussed in Sect. 4.1.1. In case of Fe-promoted Mo/HZSM-5, no significant agglomeration was observed and the conversion of CH_4 increased with increase in Fe loading (Sect. 4.1.1). Moreover, in Fe-promoted Mo/HZSM-5 catalyst, carbon nanostructures were formed, and the diameter of the carbon nanostructures increased with increasing Fe loading. These carbon nanostructures were not found in unmodified or K and Rh promoted Mo/HZSM-5 spent catalysts. Thus, Fe as a promotor in Mo/HZSM-5 facilitated the formation of carbon nanostructures as reported by the studies of Xu et al. [27, 35, 36].

4.4 Temperature Programmed Oxidation Of Spent Catalysts

Figure 11 shows the temperature programmed oxidation of spent catalysts subjected to MDA at 750 °C. The DTA curves show four regions in the TPO profile. In region I, before 350 °C, there was no significant weight change as the samples were dried at 350 °C in He. In region II, between 380 and 480 °C, considerable increase in weight was observed, corresponding to the oxidation of molybdenum carbide to molybdenum oxide [32]. In region III, between 500 and 700 °C, significant weight loss was observed in all the catalysts, attributed to the removal of coke. In case of Mo/HZSM-5 and K-Mo/HZSM-5, two distinct weight loss peaks around 510 °C and 580 °C were observed. The low temperature peak around 510 °C corresponds to removal of hydrogenated carbon species and the high temperature peak around 580 °C corresponds to the removal of hydrogen deficient carbon deposits [39]. In case of Rh-Mo/HZSM-5, a single weight loss peak around 525 °C was seen. The high temperature peak attributed to the hydrogen deficient carbon species was not present for this catalyst. As for the Fe-Mo/HZSM-5, the low temperature peak was not well distinguished from the high temperature peak and the peak corresponding to maximum weight loss was observed around 610 °C. This peak was attributed to the removal of carbon nanostructures formed during the methane activation as reported by Xu et al. [36]. In region IV, around 715 °C, a

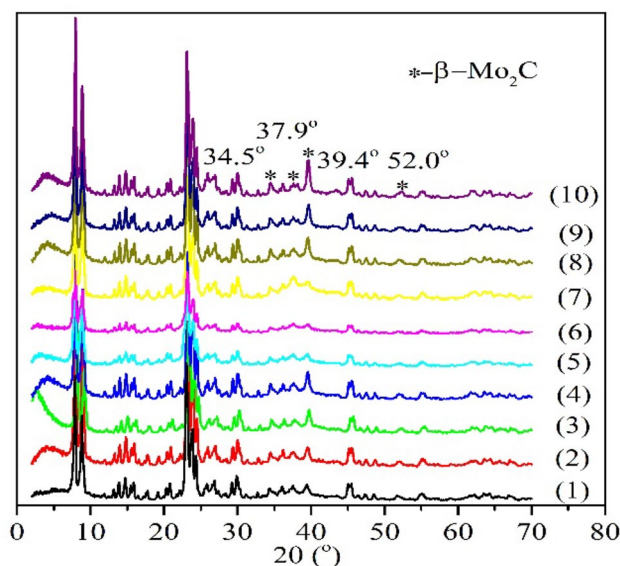


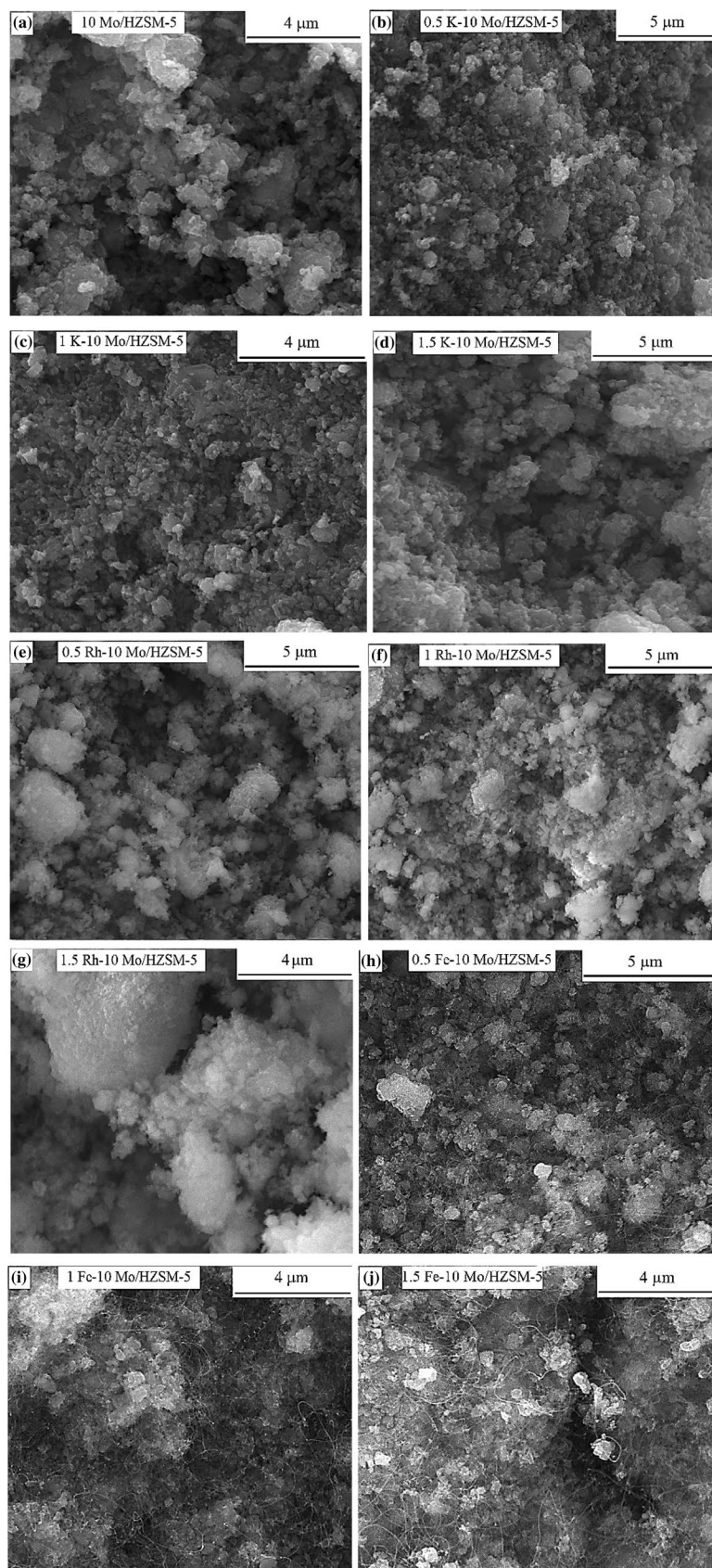
Fig. 9 XRD patterns of spent catalyst (1) 10 wt% Mo/HZMS-5 (2) 0.5 K-10 Mo/HZSM-5 (3) 1 K-10 Mo/HZSM-5 (4) 1.5 K-10 Mo/HZSM-5 (5) 0.5 Rh-10 Mo/HZSM-5 (6) 1 Rh-10 Mo/HZSM-5 (7) 1.5 Rh-10 Mo/HZSM-5 (8) 0.5 Fe-10 Mo/HZSM-5 (9) 1 Fe-10 Mo/HZSM-5 (10) 1.5 Fe-10 Mo/HZSM-5

weight loss peak possibly attributed to the sublimation of Mo species was observed. Table 4 shows the relative weight loss of the catalyst due to the removal of carbon and it was evident that the least amount of coking was observed over the surface of K-Mo/HZSM-5. The Fe-promoted catalyst showed significant weight loss due to the removal of carbon nanostructures.

5 Conclusion

MDA studies over H_2 reduced, K, Rh and Fe-promoted Mo/HZMS-5 catalysts revealed that increasing the Fe loading improved the CH_4 conversion whereas increasing the K and Rh loading decreased the conversion of CH_4 when compared to Mo/HZSM-5. When the catalysts were reduced in H_2 before methane activation, no significant change was observed in the phase of active sites (Mo_2C) formed in K, Rh and Fe-promoted catalyst when compared to Mo/HZSM-5. The K-promoted Mo/HZSM-5 catalysts exhibited better selectivity for C2 hydrocarbon and C_6H_6 compared to all other catalysts. Rh-promoted catalyst prepared by sequential impregnation exhibited poor catalytic activity for CH_4 conversion and C_6H_6 selectivity. Fe-promoted catalyst enhanced the CH_4 conversion but the selectivity of C_6H_6 declined significantly in the presence of Fe. Compared to Mo/HZMS-5, K and Rh-promoted catalysts reduced the carbon deposition on the catalyst, but Fe enhanced the formation of carbon species. The improved selectivity of C2 and C_6H_6 with less

Fig. 10 SEM images of spent catalysts of **a** 10 wt% Mo/HZSM-5 **b** 0.5 K-10 Mo/HZSM-5 **c** 1 K-10 Mo/HZSM-5 **d** 1.5 K-10 Mo/HZSM-5 **e** 0.5 Rh-10 Mo/HZSM-5 **f** 1 Rh-10 Mo/HZSM-5 **g** 1.5 Rh-10 Mo/HZSM-5 **h** 0.5 Fe-10 Mo/HZSM-5 **i** 1 Fe-10 Mo/HZSM-5 **j** 1.5 Fe-10 Mo/HZSM-5



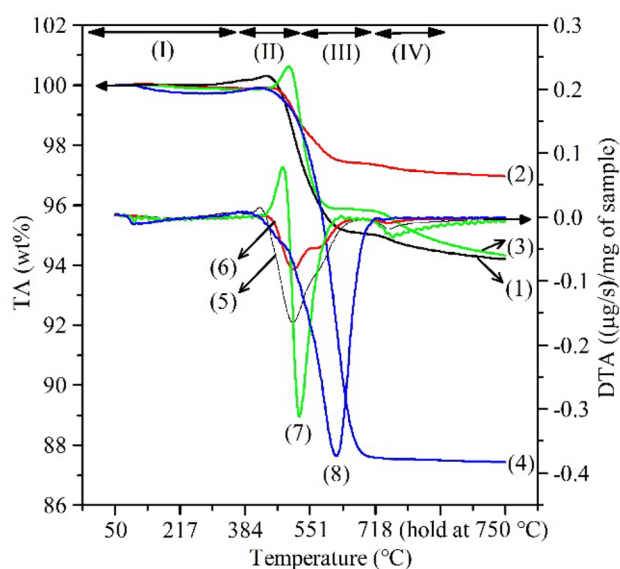


Fig. 11 TPO profiles of 10 wt% Mo/HZSM-5 [(1) TA, (5) DTA], 1.5 K-10 Mo/HZSM-5 [(2) TA, (6) DTA], 1.5 Rh-10 Mo/HZSM-5 [(3) TA, (7) DTA] and 1.5Fe-10 Mo/HZSM-5 [(4) TA, (8) DTA]

Table 4 Weight loss of catalysts during TPO studies

Catalyst	10 Mo/ HZSM-5	1.5K-10 Mo/HZSM- 5	1.5 Rh-10 Mo/HZSM- 5	1.5 Fe-10 Mo/HZSM-5
Weight loss (%)	5.81	3.04	5.68	12.56

coke formation by K-promoted catalyst is possibly due to the promotional effect of K which modified the H^+ sites (acidic strength of the catalyst) and restricted the agglomeration of heavier molecules like C_6H_6 to form coke. Though addition of K improved the selectivity of desired product and reduced catalytic coking, increasing the K loading suppressed the conversion of CH_4 . Thus, in K-promoted catalyst there exists a trade-off between catalytic activity for CH_4 conversion and improving the selectivity of C_6H_6 while decreasing the coke formation.

Acknowledgements The financial support from the University of Tulsa (Faculty Development Summer Fellowship) and ACS-PRF (PRF# 56052-DNI9) are gratefully acknowledged. We thank Dr. Winton Cornell, Applied Associate Professor, The University of Tulsa, for the XRD measurements.

Compliance of Ethical Standards

Conflict of interest The authors declare that they have no conflict of interest.

References

- Xu Y, Bao X, Lin L (2003) *J Catal* 216:386–395
- Rostrup-Nielsen JR, Sehested J, Nørskov JK (2002) *Adv Catal* 47:65–139
- Wang L, Tao L, Xie M, Xu G, Huang J, Xu Y (1993) *Catal Lett* 21:35–41
- Chen L, Lin L, Xu Z, Li X, Zhang T (1995) *J Catal* 157:190–200
- Liu B, Zhang Y, Liu J, Tian M, Zhang F, Au C, Cheung A-C (2011) *J Phys Chem C* 115:16954–16962
- Xiong Z-T, Zhang H-B, Lin G-D, Zeng J-L (2001) *Catal Lett* 74:233–239
- Zeng JL, Xiong ZT, Zhang HB, Lin GD, Tsai K (1998) *Catal Lett* 53:119–124
- Wang L, Ohnishi R, Ichikawa M (2000) *J Catal* 190:276–283
- Shen XC, Lou H, Hu K, Zheng XM (2007) *Chin Chem Lett* 18:479–482
- Zhang C-L, Li S, Yuan Y, Zhang W-X, Wu T-H, Lin L-W (1998) *Catal Lett* 56:207–213
- Wong S-T, Xu Y, Liu W, Wang L, Guo X (1996) *Appl Catal A* 136:7–17
- Wu P, Kan Q, Wang D, Xing H, Jia M, Wu T (2005) *Catal Commun* 6:449–454
- Wang D, Kan Q, Xu N, Wu P, Wu T (2004) *Catal Today* 93:75–80
- Ma D, Shu Y, Han X, Liu X, Xu Y, Bao X (2001) *J Phys Chem B* 105:1786–1793
- Ding W, Meitzner GD, Iglesia E (2002) *J Catal* 206:14–22
- Li Y, Liu L, Huang X, Liu X, Shen W, Xu Y, Bao X (2007) *Catal Commun* 8:1567–1572
- Zhu P, Yang G, Sun J, Fan R, Zhang P, Yoneyama Y, Tsubaki N (2017) *J Mater Chem A* 5:8599–8607
- Zhang Y, Jiang H (2018) *Chem Commun* 54:10343–10346
- Ma H, Kojima R, Kikuchi S, Ichikawa M (2005) *Catal Lett* 104:63–66
- Ohnishi R, Liu S, Dong Q, Wang L, Ichikawa M (1999) *J Catal* 182:92–103
- Lacheen HS, Iglesia E (2005) *J Catal* 230:173–185
- Liu Z, Nutt MA, Iglesia E (2002) *Catal Lett* 81:271–279
- Tan P (2018) *Catal Commun* 103:101–104
- Burns S, Hargreaves J, Pal P, Parida K, Parija S (2006) *Catal Today* 114:383–387
- Rodrigues ACC, Monteiro JLF (2008) *Catal Commun* 9:1060–1065
- Dong Q, Zhao X, Wang J, Ichikawa M (2004) *J Nat Gas Chem* 13:36–40
- Xu Y, Wang J, Suzuki Y, Zhang Z-G (2012) *Catal Today* 185:41–46
- Masiero SS, Marcilio NR, Perez-Lopez OW (2009) *Catal Lett* 131:194–202
- Aboul-Gheit AK, Awadallah AE, Aboul-Enein AA, Mahmoud A-LH (2011) *Fuel* 90:3040–3046
- Liu B, Yang Y, Sayari A (2001) *Appl Catal A* 214:95–102
- Tshabalala TE, Coville NJ, Scurrrell MS (2014) *Appl Catal A* 485:238–244
- Cheng X, Yan P, Zhang X, Yang F, Dai C, Li D, Ma X-X (2017) *Mol Catal* 437:114–120
- Iliuta MC, Iliuta I, Grandjean BP, Larachi F (2003) *Ind Eng Chem Res* 42:3203–3209
- Larachi F, Oudghiri-Hassani H, Iliuta M, Grandjean B, McBreen P (2002) *Catal Lett* 84:183–192
- Xu Y, Wang J, Suzuki Y, Zhang Z-G (2011) *Appl Catal A* 409:181–193
- Xu Y, Suzuki Y, Zhang Z-G (2013) *Appl Catal A* 452:105–116

37. Sun K, Gong W, Gasem K, Adidharma H, Fan M, Chen R (2017) *Ind Eng Chem Res* 56:11398–11412
38. Sun K, Ginosar DM, He T, Zhang Y, Fan M, Chen R (2018) *Ind Eng Chem Res* 57:1768–1789
39. Abdelsayed V, Shekhawat D, Smith MW (2015) *Fuel* 139:401–410
40. Aboul-Gheit AK, El-Masry MS, Awadallah AE (2012) *Fuel Process Technol* 102:24–29
41. Xiong Z-T, Chen L-L, Zhang H-B, Zeng J-L, Lin G-D (2001) *Catal Lett* 74:227–232
42. Tshabalala TE, Coville NJ, Anderson JA, Scurrell MS (2015) *Appl Catal A* 503:218–226
43. Pinglian T, Zhusheng X, Tao Z, Liayuan C, Liwu L (1997) *React Kinet Catal Lett* 61:391–396
44. Liu B, Jiang L, Sun H, Au C (2007) *Appl Surf Sci* 253:5092–5100
45. Shu Y, Xu Y, Wong S-T, Wang L, Guo X (1997) *J Catal* 170:11–19
46. Martínez A, Peris E (2016) *Appl Catal A* 515:32–44
47. Wang L, Xu Y, Wong S-T, Cui W, Guo X (1997) *Appl Catal A* 152:173–182
48. Kojima R, Kikuchi S, Ma H, Bai J, Ichikawa M (2006) *Catal Lett* 110:15–21
49. Ramasubramanian V, Ramsurn H, Price GL, J. *Energy Chem.* (2018)
50. Price GL, Kanazirev V (1997) *Zeolites* 18:33–37
51. Kanazirev VI, Price GL, Dooley KM (1994) *J Catal* 148:164–180
52. Kanazirev V, Dooley KM, Price GL (1994) *J Catal* 146:228–236
53. Lee JS, Lee KH, Lee JY (1992) *J Phys Chem* 96:362–366
54. Scurrell M (1987) *Appl Catal* 32:1–22
55. Scurrell M (1988) *Appl Catal* 41:89–98
56. Oshikawa K, Nagai M, Omi S (2001) *J Phys Chem B* 105:9124–9131

Publisher's Note Springer Nature remains neutral with regard to jurisdictional claims in published maps and institutional affiliations.